DOI: 10.1002/adma.200600675

Reduction by the End Groups of Poly(vinyl pyrrolidone): A New and Versatile Route to the Kinetically Controlled Synthesis of Ag Triangular Nanoplates**

By *Isao Washio*, *Yujie Xiong*, *Yadong Yin*, and *Younan Xia**

Polymers are widely used in the chemical synthesis of colloidal nanocrystals, and their roles are generally documented as steric stabilizers or capping agents.[1,2] In particular, poly(vinyl pyrrolidone) (PVP) has received special attention because of its high chemical stability, nontoxicity, and excellent solubility in many polar solvents.[1,2] Although the repeating unit of PVP has been extensively investigated for its coordination capability, the end groups of PVP remain largely unexplored in terms of functionality and reactivity. For commercially available PVP, their ends are terminated with the hydroxyl (–OH) group because of the involvement of water as a polymerization medium and the presence of hydrogen peroxide. Like long-chain alcohols, we suspect that such polymers can serve as a new class of reductants, whose mild reducing power is desired for kinetically controlled synthesis of metal nanocrystals. As established for a number of systems, kinetic control provides a simple and versatile route to the synthesis of metal nanocrystals with well-defined shapes.[3] For a face-centered cubic (fcc) noble metal, the thermodynamically favorable shapes are truncated nanocubes and multiple twinned particles (MTPs).[2] When metal atoms are generated at a sufficiently high rate, the final product will have no choice but to take the thermodynamically favored shapes. As the reduction becomes substantially slower, however, the nucleation and growth will be turned into kinetic control and the final product can take a range of shapes that deviate from the thermodynamic ones. Here we demonstrate for the first time that the reduction kinetics of $AgNO_3$ by the hydroxyl end group of PVP can be maneuvered in at least two different ways to produce Ag triangular nanoplates in high yields.

Silver nanostructures have especially been of interest because of their unique surface-plasmonic features, which have enabled their use as optical labels, active substrates for surface-enhanced Raman scattering (SERS), near-field optical probes, and contrast agents for biomedical imaging.[4] Like many other systems, shape control has received considerable attention for silver,[1c,2,5,6] because in many cases it allows one to tune the properties for various applications with a greater versatility than can be achieved otherwise.[5,7,8] Most recently, particular emphasis has been placed on triangular nanoplates, as metal nanostructures with sharp corners and edges are capable of generating maximum electromagnetic-field enhancement and thus make these nanoparticles attractive as substrates for SERS detection or other spectroscopic techniques.[9] Although several research groups have developed diverse methods to generate triangular and circular nanoplates of Ag in a number of different solvents,[1c,6,10] the ability to control and fine-tune the shape of Ag nanostructures has been modestly successful. It still remains a grand challenge to produce Ag triangular nanoplates with controllable size in bulk quantities and with high yield via a facile and clean method. In this communication, Ag nanoplates between 50 and 350 nm in size were synthesized by heating an aqueous solution of $AgNO_3$ and PVP in a capped vial, in which the reduction kinetics and growth were significantly altered towards the thin-plate morphology.

Figure 1a–e shows scanning electron microscopy (SEM) images of samples taken at different stages from a synthesis where the molar ratio of PVP (weight-average molecular weight $M_w = 29\,000$ g mol^{-1}, calculated in terms of the repeating unit) to $AgNO_3$ was 30. As shown in Figure S1 in the Supporting Information, the sample contained 80 % circular nanoplates 50 nm in size and 20 % spherical nanoparticles 20 nm in size at synthesis time $t = 20$ min. At $t = 40$ min (Fig. 1a), the average size of the circular nanoplates and spherical nanoparticles grew to 60 and 25 nm, respectively. The inset in Figure 1a shows an SEM image of tilted circular nanoplates, revealing their thickness as ca. 5 nm. As the reaction proceeded, the circular shape of nanoplates gradually

[*] Prof. Y. Xia, I. Washio, Dr. Y. Xiong
Department of Chemistry, University of Washington
Seattle, WA 98195 (USA)
E-mail: xia@chem.washington.edu
Dr. Y. Yin
The Molecular Foundry, Lawrence Berkeley National Laboratory
Berkeley, CA 94720 (USA)

[**] This work was supported in part by a grant from the NSF (DMR-0451788), a subcontract from the NSF-funded MERSEC program awarded to the UW, and a fellowship from the David and Lucile Packard Foundation. Y. X. is a Camille Dreyfus Teacher Scholar (2002–2007). I. W. was a visiting student from Tokyo Institute of Technology and partially supported by a research fellowship from the Japan Society for the Promotion of Science (JSPS) for Young Scientists. Y. Y. was supported by the Director, Office of Science, U.S. Department of Energy, under Contract DE-AC03-76SF00098. This work used the Nanotech User Facility (NTUF) at UW, a member of the National Nanotechnology Infrastructure Network (NNIN) funded by the NSF. We thank the Molecular Foundry at the Lawrence Berkeley National Laboratory for HRTEM analysis. Supporting Information is available online from Wiley InterScience or from the author.

ADVANCED MATERIALS

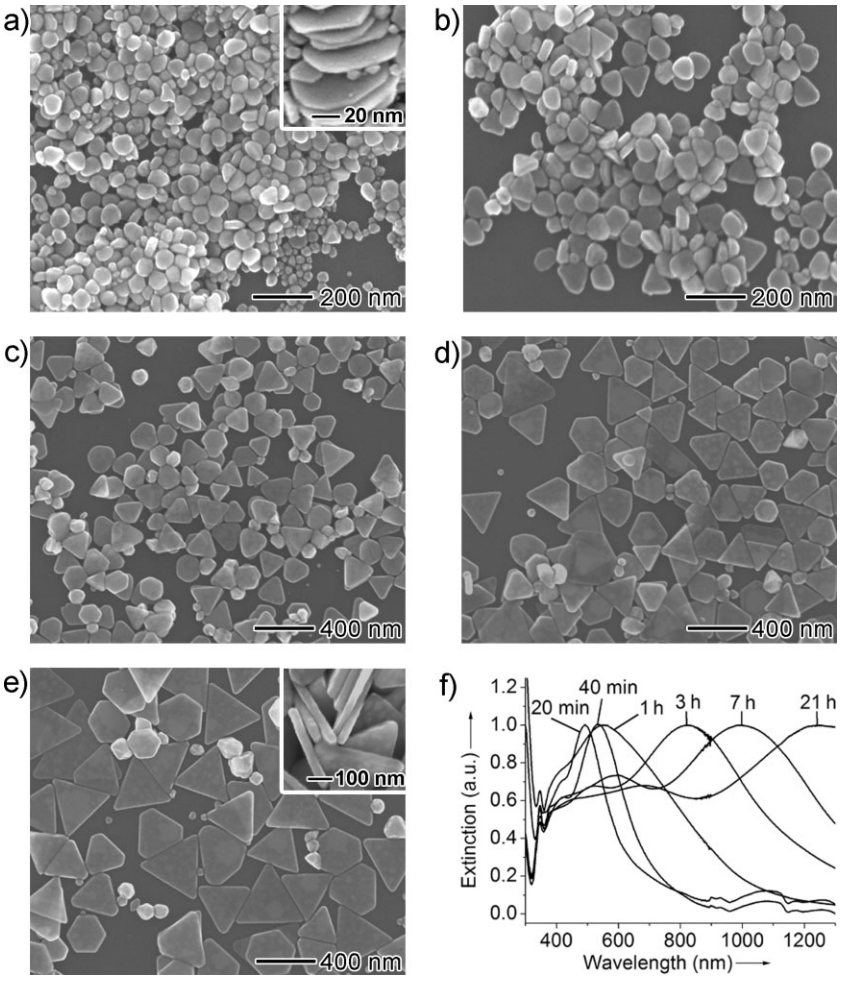

Figure 1. SEM images of products sampled at different stages of a synthesis: a) $t = 40$ min, b) $t = 1$ h; c) $t = 3$ h; d) $t = 7$ h; and e) $t = 21$ h. f) UV-vis spectra of these products dispersed in water. The insets of (a) and (e) are SEM images taken from tilted samples. The PVP had an average molecular weight of 29 000 g mol^{-1} and its molar ratio (in terms of the repeating unit) to $AgNO_3$ was 30.

evolved into faceted ones with sharp edges and corners. At $t = 1$ h (Fig. 1b), the sample consisted of triangular nanoplates of 90 nm in edge length and spherical nanoparticles 35 nm in size. The lateral dimensions of both nanoplates and nanoparticles continued to increase with reaction time. At $t = 3$ h (Fig. 1c), the triangular nanoplates and nanoparticles increased in size to 170 and 80 nm, respectively. In the following 4 h, most of the triangular nanoplates grew to 250 nm in edge length, together with a small portion of nanoparticles 100 nm in size (Fig. 1d and Fig. S2a). Both nanoplates and nanoparticles grew slowly during the next 14 h. As shown in Figures 1e and S2b, at $t = 21$ h, the size of nanoplates and nanoparticles became 350 and 120 nm, respectively. For the nanoplates, the ratio of thickness to edge length was ca. 0.12 (see the inset in Fig. 1e). It is worth noting that the ratio between the numbers of nanoplates and nanoparticles was essentially unchanged during the entire growth process .

We further characterized the shape and structure of the product using transmission electron microscopy (TEM). Figure 2a shows a TEM image of spherical particles in the sample depicted in Figure 1b ($t = 1$ h), indicating that the spherical nanoparticles of relatively small size were multiply twinned. The inset in Figure 2a gives an electron-diffraction pattern taken from the twinned particle. The rings correspond to diffraction from the {111}, {200}, {220}, and {311} planes of fcc Ag. Figure 2b shows a high-resolution TEM image of the nanoplate recorded along the [$\bar{1}$11] zone axis. The fringes are separated by 2.5 Å, which can be ascribed to the (1/3){422} reflection that is generally forbidden for an fcc lattice. The inset in Figure 2b shows a typical electron diffraction pattern recorded by directing the electron beam perpendicular to the triangular flat faces of an individual nanoplate. The sixfold rotational symmetry displayed by the diffraction spots implies that the triangular faces are presented by {111} planes. Three sets of spots can be identified based on the *d*-spacing: the set with a spacing of 1.4 Å results from the {220} reflection of fcc Ag. The outer set with a lattice spacing of 0.8 Å can be indexed to the {422} Bragg reflection. These two sets of reflection were both allowed by an fcc lattice. The inner set with a spacing of 2.5 Å is believed to originate from the forbidden (1/3){422} reflection. This forbidden reflection has also been previously observed for Ag or Au nanostructures in the form of thin plates or films bounded by atomically flat surfaces.[1c,6,10,11] This assignment is consistent with the geometrical model, in which each triangular nanoplate is bound by two {111} planes as the top and bottom faces and three {100} planes as the side faces.[12]

The edge length of the nanoplates can be readily controlled by adjusting the reaction time. It is worth pointing out that the samples displayed size-dependent surface plasmon resonance (SPR) properties. Figure 1f shows UV-vis extinction spectra of aqueous suspensions of Ag particles obtained at different stages of the reaction. The extinction peaks at 490, 530, 550, 820, 1000, and 1240 nm can be attributed to the in-plane dipole resonance of nanoplates, while the shoulders at 390–400, 510, 590, and 690 nm correspond to their out-of-plane resonance. Similar to previous publications, the positions of the extinction peaks were gradually red-shifted to the near-IR region of the electromagnetic spectrum with increasing particle size, exhibiting a strong size dependence for the SPR bands.

To determine the role of PVP in the reaction, we conducted a series of syntheses by varying the molar ratio of PVP to $AgNO_3$ as well as the molecular weight of PVP. As shown in

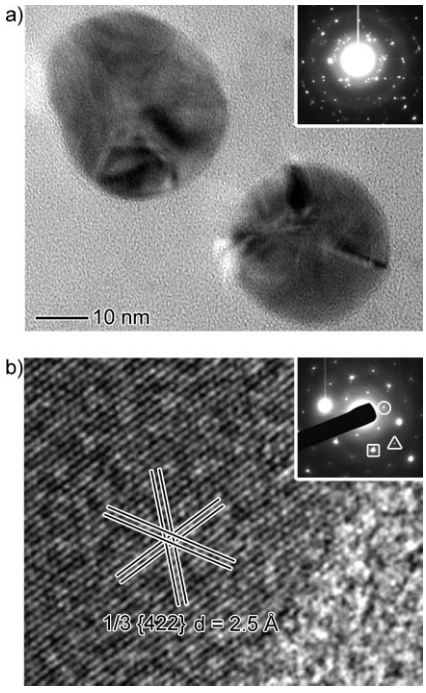

Figure 2. a) TEM image of two multiply twinned particles in the sample shown in Figure 1b (t = 1 h). b) High-resolution TEM images of the edge of a triangular nanoplate in the sample shown in Figure 1b (t = 1 h). The insets show the electron diffraction patterns taken from a single twinned particle and a triangular nanoplate, respectively. For the nanoplate, the strongest spots (square) could be indexed to the allowed {220} reflection, the outer spots (triangle) with the weakest intensity could be assigned to the allowed {422} reflection, and the inner spots (circle) with a weaker intensity corresponded to the formally forbidden (1/3){422} reflection.

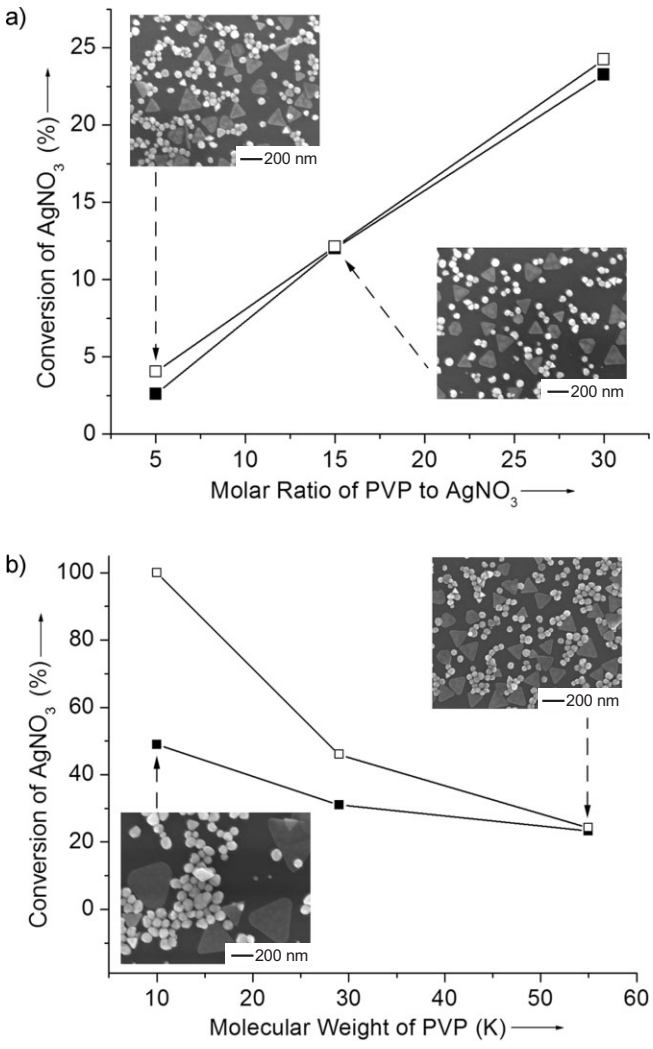

Figure 3. a) Plot showing the linear dependence of the conversion percentage of $AgNO_3$ to Ag on the molar ratio of PVP (M_w = 55 000 g mol^{-1}) to $AgNO_3$. b) Plot showing the dependence of the conversion percentage of $AgNO_3$ to Ag on the molecular weight of PVP, with the molar ratio of PVP to $AgNO_3$ being kept at 30. The solid squares represent the experimental conversion percentages measured by atomic emission spectroscopy, while the hollow boxes correspond to stoichiometric calculations. In both cases, the molar ratio of PVP to $AgNO_3$ was calculated in terms of the repeating unit. The insets show SEM images of samples synthesized under the corresponding conditions.

Figure 3a, the conversion percentage of $AgNO_3$ to Ag had a linear dependence on the molar ratio of PVP to $AgNO_3$. In contrast, the conversion percentage decreased as PVPs of higher molecular weights were used (Fig. 3b). Taken together, we conclude that the amount of $AgNO_3$ that can be reduced is directly proportional to the number of PVP chains. More specifically, the reduction should be related to the end groups of PVP. As reported in the literature, the ends of commercial PVP are terminated with the –OH group.[13] To identify the end groups of PVP used in the present work, we obtained a ^{13}C NMR spectrum (Fig. 4) from PVP with a molecular weight of 10 000 g mol^{-1}. The weak peak at 61.75 ppm can be assigned to the –OH group.[13b] Although PVP has been widely cited as a steric stabilizer or capping agent in the synthesis of various colloidal particles,[1,2] this is the first demonstration that the end groups of PVP can serve as a reducing agent for the synthesis of metal nanoparticles. When compared with the calculated results (the hollow boxes in Fig. 3), the experimental conversion percentages matched well in the range below 25 %; beyond this point, they gradually deviated from the calculated values. This deviation can probably be understood by the following argument: as the molecular weight of PVP was reduced, the reduction became much faster, and some PVP adsorbed onto the surface of rapidly formed Ag nanoplates or nanoparticles, hence losing their reduction power.

In the present synthesis, the concentration of end groups not only determined the conversion percentage of $AgNO_3$ to Ag but also affected the reduction rate. When the molar ratio of PVP to $AgNO_3$ was increased or the molecular weight of PVP was decreased, the reduction rate increased. As a result, the products displayed different morphologies, as shown in the SEM images in Figure 3. In general, faster reduction led to particles of larger size. Since the formation of triangular

ADVANCED MATERIALS

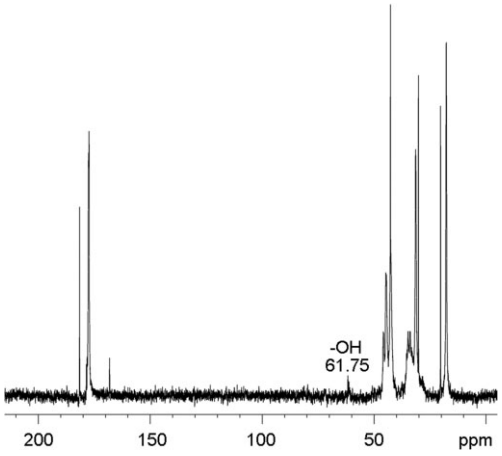

Figure 4. ^{13}C NMR spectrum of PVP ($M_w = 10\,000$ g mol^{-1}) dissolved in D_2O.

nanoplates was controlled by growth kinetics, slower reaction was advantageous for the formation of nanoplates at higher yields. With regard to size uniformity, the reduction rate should be kept moderate, as an extremely slow reaction would continue generating Ag atoms, which eliminated the Ostwald ripening and thus resulted in size polydispersity. For the current synthesis, Figure 1 presents the optimized conditions: use of 29 000 g mol^{-1} PVP with its molar ratio to $AgNO_3$ being controlled at 30.

The formation of circular and triangular Ag nanoplates can be attributed to the mild reducing power of PVP, which is associated with a slow reduction rate. Compared to truncated nanocubes and multiply twinned particles (the thermodynamically favored shapes), the surface energy of nanoplates is much higher so that their formation requires kinetic control. As the reduction was substantially slower, both nucleation and growth turned into kinetic control; the seeds with stacking faults formed at the initial nucleation stage and then grew into nanoplates that deviated from the thermodynamic structures. Note that the stacking faults are the critical characteristics for the growth of Ag and Au lamellar nanoplates.[11,14] In contrast, if the reduction rate was too fast, these seeds with defects could also evolve into other structures instead of nanoplates. Undoubtedly, as demonstrated in this paper, the slow reduction rate derived from the mild reducing power of PVP was the key to achieving the kinetically controlled synthesis of Ag nanoplates. Previously we have employed such a kinetic control to achieve the synthesis of Pd triangular and hexagonal nanoplates by coupling oxidative etching with polyol reduction.[3a] For Ag nanoplates, a number of methods have been demonstrated, including photo- or thermally induced transformation and chemical reduction.[6,10] It is worth noting that most of these methods involved Ostwald ripening that was slow enough to ensure kinetic control.[6a–c,10] The route presented here is new, versatile, and capable of producing Ag nanoplates with controllable sizes and at high yields.

In the previously reported synthesis of Ag nanoplates, light of appropriate wavelengths were indispensable for the formation of plate morphology.[6,10] To clarify this point, we performed a reaction where light was completely blocked from the reaction system. Figure S3 shows a typical SEM image of the sample prepared in the absence of light, in which we cannot find any distinct morphological differences compared with the normal synthesis (Fig. 1e). This result suggests that light is not indispensable for the formation of the thin-plate morphology.

In summary, Ag triangular nanoplates have been synthesized with high purity by heating an aqueous solution of $AgNO_3$ and PVP to 60 °C in a capped vial. The hydroxyl end groups of PVP reduced $AgNO_3$ at a sufficiently slow rate so that the growth of Ag nanocrystals became kinetically controlled, leading to the formation of triangular plates. This kinetically controlled synthesis allows one to obtain Ag nanoplates with controllable edge lengths by varying the reaction time. Although the present work was focused on silver and PVP, we believe that this new strategy can also be extended to other noble metals and many other polymers. We anticipate that reduction of metal salts by the end groups of polymers may provide a generic route to the synthesis of metal nanocrystals with controllable shapes, at high yields, and in large quantities.

Experimental

In each synthesis, poly(vinyl pyrrolidone) (PVP, Aldrich, $M_w = 10\,000$, 29 000, or 55 000 g mol^{-1}) was dissolved in 8.0 mL of water in a 20 mL vial (liquid scintillation vial with a polyethylene liner, Research Products International Corp.), and heated to 60 °C in air under magnetic stirring. Meanwhile, 3.0 mL of an aqueous solution of $AgNO_3$ (188 mM, Aldrich) was rapidly added into the vial. For PVP of each molecular weight, the molar ratio between the repeating unit of PVP and $AgNO_3$ was varied from 30, through 15, to 5. After the vial had been capped, the reaction mixture was heated at 60 °C in air for 21 h. At different stages of the reaction, samples were taken from the mixture using a glass pipette, centrifuged, and then washed with water several times to remove excess PVP. In another approach, a number of reactions were carried out under the same conditions but stopped after different periods of time. The samples were characterized by SEM, TEM, and high-resolution TEM. UV-vis extinction spectra were also taken from aqueous suspensions of the products. The water used in all steps was obtained by filtering through Millipore cartridges (E-pure, Dubuque, IA).

A drop of the aqueous suspension of silver nanoparticles was placed on a piece of silicon wafer or carbon-coated copper grid (Ted Pella, Redding, CA, for TEM) and dried under ambient conditions for SEM or TEM characterization. TEM images were captured using a Phillips 420 transmission electron microscope operated at 120 kV. HRTEM images and electron diffraction patterns were taken on a JEOL 2010 LaB_6 high-resolution transmission electron microscope operated at 200 kV. SEM images were taken on an FEI field-emission scanning electron microscope (Sirion XL) operated at an accelerating voltage of 20 kV. UV-vis spectra were recorded at room temperature on a Cary 5E (Varian) spectrophotometer using polymethacrylate cuvettes (Fisher Scientific, Pittsburgh, PA) with an optical path of 1 cm. ^{13}C NMR spectra of PVP were obtained using a Bruker AVANCE AV NMR spectrometer operated at 300.13 MHz with D_2O as the solvent. The conversion percentages of $AgNO_3$ to Ag were determined

by atomic emission spectroscopy (AES). The AES measurements were performed on a Jarrell-Ash 955 Plasma AtomComp atomic emission spectrometer. The Ag nanoparticles were collected by centrifugation after reaction and then dissolved in an aqueous HNO_3 solution (63 %). The solution was diluted to 10 ppm and then used for AES measurements. The emission line at 328.0 nm was used to measure the concentration of Ag atoms. The conversion percentage was calculated based on the amount of Ag atoms contained in the HNO_3 solution and the amount of $AgNO_3$ in the starting solution.

Received: March 29, 2006
Published online: June 8, 2006

[1] a) D. G. Duff, A. Baiker, P. Edwards, *Langmuir* **1993**, *9*, 2301. b) P. Y. Agt, R. H. Urbina, K. T. Elhsissen, *J. Mater. Chem.* **1997**, *7*, 293. c) I. Pastoriza-Santos, L. M. Liz-Marzán, *Nano Lett.* **2002**, *2*, 903. d) J. Chen, T. Herricks, M. Geissler, Y. Xia, *J. Am. Chem. Soc.* **2004**, *126*, 10 854. e) Y. Xiong, J. Chen, B. Wiley, Y. Xia, S. Aloni, Y. Yin, *J. Am. Chem. Soc.* **2005**, *127*, 7332.

[2] a) Y. Sun, Y. Xia, *Science* **2002**, *298*, 2176. b) B. Wiley, T. Herricks, Y. Sun, Y. Xia, *Nano Lett.* **2004**, *4*, 1733. c) B. Wiley, Y. Sun, B. Mayers, Y. Xia, *Chem. Eur. J.* **2005**, *11*, 455.

[3] a) Y. Xiong, J. M. McLellan, J. Chen, Y. Yin, Z.-Y. Li, Y. Xia, *J. Am. Chem. Soc.* **2005**, *127*, 17 118. b) J. Chen, T. Herricks, Y. Xia, *Angew. Chem. Int. Ed.* **2004**, *44*, 2589.

[4] a) S. Nie, S. R. Emory, *Science* **1997**, *275*, 1102. b) O. D. Velve, E. W. Kaler, *Langmuir* **1999**, *15*, 3693. c) S. R. Nicewarner-Peña, R. G. Freeman, B. D. Reiss, L. He, D. J. Peña, I. D. Walton, R. Cromer, C. D. Keating, M. J. Natan, *Science* **2001**, *294*, 137. d) Y. C. Cao, R. Jin, C. A. Mirkin, *Science* **2002**, *297*, 1536. e) L. A. Dick, A. D. McFarland, C. L. Haynes, R. P. Van Duyne, *J. Phys. Chem. B* **2002**, *106*, 853. f) A. P. Alivisatos, *Nat. Biotechnol.* **2004**, *22*, 47.

[5] a) C. J. Murphy, N. R. Jana, *Adv. Mater.* **2002**, *14*, 80. b) K. K. Caswell, J. N. Wilson, U. H. F. Bunz, C. J. Murphy, *J. Am. Chem. Soc.* **2003**, *125*, 13 914. c) S. H. Im, Y. T. Lee, B. Wiley, Y. Xia, *Angew. Chem. Int. Ed.* **2005**, *44*, 2154. d) D. Yu, V. W.-W. Yam, *J. Am. Chem. Soc.* **2004**, *126*, 13 200.

[6] a) S. Chen, D. L. Carroll, *Nano Lett.* **2002**, *2*, 1003. b) S. Chen, Z. Fan, D. L. Carroll, *J. Phys. Chem. B* **2002**, *106*, 10 777. c) D. O. Yener, J. Sindel, C. A. Randall, J. H. Adair, *Langmuir* **2002**, *18*, 8692. d) M. Maillard, S. Giorgio, M.-P. Pileni, *Adv. Mater.* **2002**, *14*, 1084.

[7] a) U. Kreibig, M. Vollmer, *Optical Properties of Metal Clusters*, Springer, New York **1995**. b) M. A. El-Sayed, *Acc. Chem. Res.* **2001**, *34*, 257. c) J. B. Jackson, N. J. Halas, *J. Phys. Chem. B* **2001**, *105*, 2473.

[8] a) T. R. Jensen, L. Kelly, A. Lazarides, G. C. Schatz, *J. Cluster Sci.* **1999**, *10*, 295. b) J. P. Kottmann, O. J. F. Martin, D. R. Smith, S. Schultz, *Phys. Rev. B: Condens. Matter Mater. Phys.* **2001**, *64*, 235 402. c) M. Muniz-Miranda, *Chem. Phys. Lett.* **2001**, *340*, 437. d) I. O. Sosa, C. Noguez, R. G. Barrera, *J. Phys. Chem. B* **2003**, *107*, 6269.

[9] a) W. H. Yang, G. C. Schatz, R. P. Van Duyne, *J. Chem. Phys.* **1995**, *103*, 869. b) K. L. Kelly, E. Coronado, L. L. Zhao, G. C. Schatz, *J. Phys. Chem. B* **2003**, *107*, 668.

[10] a) R. Jin, Y. Cao, C. A. Mirkin, K. L. Kelly, G. C. Schatz, J. G. Zheng, *Science* **2001**, *294*, 1901. b) R. Jin, Y. C. Cao, E. Hao, G. S. Metraux, G. C. Schatz, C. A. Mirkin, *Nature* **2003**, *425*, 487. c) Y. Sun, Y. Xia, *Adv. Mater.* **2003**, *15*, 695. d) Y. Sun, B. Mayers, Y. Xia, *Nano Lett.* **2003**, *3*, 675.

[11] a) A. I. Kirkland, D. A. Jefferson, D. G. Duff, P. P. Edwards, I. Gameson, B. F. G. Johnson, D. J. Smith, *Proc. R. Soc. London, Ser. A* **1993**, *440*, 589. b) V. Germain, J. Li, D. Ingert, Z. L. Wang, M. P. Pileni, *J. Phys. Chem. B* **2003**, *107*, 8717.

[12] Z. L. Wang, *J. Phys. Chem. B* **2000**, *104*, 1153.

[13] a) W. Reppe, *Polyvinylpyrrolidon*, VCH, Weinheim, Germany **1954**. b) K. Raith, A. V. Kühn, F. Rosche, R. Wolf, R. H. H. Neubert, *Pharm. Res.* **2002**, *19*, 556.

[14] C. Lofton, W. Sigmund, *Adv. Funct. Mater.* **2005**, *15*, 1197.

